Duct noise attenuation using reactive silencer with various internal configurations

Xiang Yu and Li Cheng[*]

Department of Mechanical Engineering, The Hong Kong Polytechnic University,

Hung Hom, Kowloon, Hong Kong, SAR of China

li.cheng@polyu.edu.hk

Abstract

The broadband sound attenuation characteristics of expansion chamber silencers can be altered by their internal configuration. Three-dimensional modeling of such systems, especially in the presence of complex internal partitions, remains a challenging task. In order to tackle the system complexity, this paper presents a systematic approach based on the sub-structuring modeling principle, to investigate the effects of several typical silencer configurations and provide guidelines for possible system optimization. Through numerical examples, the effects of various internal arrangements, including the side-branch partitions, multi-chamber partitions, non-symmetric inlet/outlet, and their combined effects are investigated. Numerical predictions show good agreements with both finite element method (FEM) and experiments. Investigations suggest some critical issues and possible solutions for better silencer design.

Keywords: Expansion chamber; Reactive silencer; Transmission loss; Internal partition; Muffler design.

1. Introduction

Noise attenuation inside a duct is an important topic of practical interest. Typical examples are pumps and compressors, induction and discharging pipes, engine exhausts, building ventilation systems, etc. Among various passive noise control measures, expansion chamber silencers [1] have been widely used due to their relatively simple structure and broadband sound attenuation characteristics. The well-known dome-like behavior in the transmission loss (TL) curve, however, neutralizes the silencing effect at the troughs, and the overall attenuation performance is limited by the expansion ratio that can practically be achieved. Moreover, a simple expansion chamber usually has the drawback of inducing high pressure drop due to the sudden cross-sectional change at the expansion and contraction.

In dealing with the above constraints, reactive silencers with various internal configurations have been investigated in the literature [2-9]. For example, Åbom [2] proposed a general analytical approach to evaluate the four-pole parameters of an expansion chamber with extended inlet and outlet. Selamet and Ji [3] showed that the expansion chambers with inlet/outlet extensions combine the broadband domes and extra resonant peaks below the cut-off frequency, which also helps alleviate the induced pressure drop. Huang [4] developed the so-called plate silencers with side-branch cavities covered by flexible plates, which give rise to noise attenuation through wave reflection towards the upstream. The work was later on extended to sandwich plates to facilitate practical implementations [5]. Lee and Kim [6] studied the effect and optimization of additional vertical partitions inside the chamber, which

leads to an increased TL, a wider dome-type attenuation and a simultaneous enhancement of flow performance [7]. Middelberg *et al*. [8] evaluated the acoustic behavior and induced pressure drop of dual-chamber mufflers using computational fluid dynamics (CFD) analysis. Meanwhile, in the pursuit of better sound attenuation, hybrid silencers with additional dissipative elements such as sound absorption materials or perforated linings have also been investigated [10-13].

With the increasing internal structural complexities, effective modeling tools which eventually allow flexible analyses and optimizations are crucial. One-dimensional theory based on plane wave assumption is only accurate in the low frequency range before the onset of multi-dimensional waves [1]. To deal with higher-order acoustic modes, 2-D/3-D analytical approaches based on the modal matching technique have been employed, which consist in decomposing the pressure field inside each acoustic domain into oppositely propagating acoustic waves and relating the continuity conditions at the corresponding boundaries. Typical work includes circular [1, 3], multi-chamber [9], rectangular and elliptical [14] silencers. However, these approaches are confined to relatively simple configurations. When dealing with complex internal layouts with several coupled domains, the number of the continuity equations to be established drastically increases and the modeling procedure becomes very tedious. As an alternative, finite element/boundary element method (FEM/BEM) has also been frequently employed [6, 12]. Although FEM/BEM is able to cope with system complexities, it is highly computational intensive when the system dimension is large, and the convergence starts to show problem when the

frequency is high. Most importantly, FEM/BEM can hardly provide the efficiency and the flexibility needed for system optimization.

Sub-structuring techniques can possibly provide the most appropriate solution in overcoming these difficulties in the system modeling, and at the same time, offer great potential in performing system optimizations. By dissembling the global system into sub-systems, each sub-system can be characterized before they are coupled together. The assembling treatment can then be performed through rather simple continuity descriptions at the connecting interfaces, and re-calculations are required only for subsystems with changing parameters during the system optimization. When using the existing sub-structuring approaches for silencer applications with multiple internal partitions, however, the inner acoustic domains are usually connected via multiple partial structures (sometimes even flexible ones) with apertures. The co-existence of parallel structural and acoustic transmission paths restricts the straightforward coupling treatment when applying simple continuity descriptions, and thus adds tremendous difficulties to the existing sub-structuring techniques. Therefore, it is the aim of this paper to propose a general modeling framework under the sub-structuring principle, with a convenient treatment of mixed separations, to systematically tackle the complexities and difficulties involved in silencer design problems.
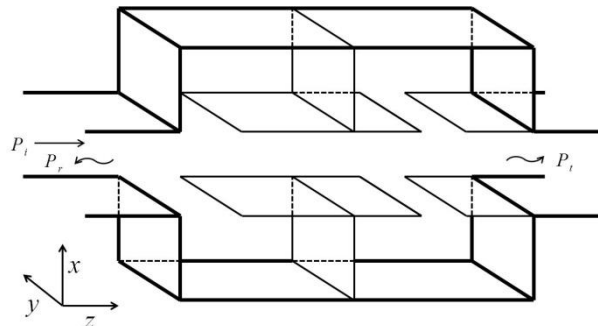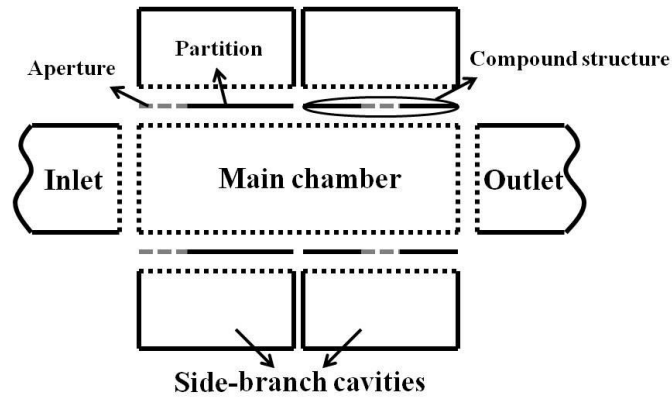
Fig. 1. (a) An example of reactive silencers with complex internal partitions (b) Using sub-structuring technique, the system is divided into uncoupled subsystems.

Figure 1(a) shows a typical example of a three-dimensional expansion chamber with complex internal configuration. In this paper, a systematic sub-structuring formulation based on the Patch Transfer Function (PTF) method [15-18] is proposed to calculate the TL, and to investigate the separate and combined effects of several typical internal arrangements on the silencing performance. The PTF approach has been demonstrated to be more computational efficient, and capable of covering a much wider frequency range (low to mid-high) than other conventional methods such as FEM/BEM [15,16]. Figure 1(b) illustrates the decoupling treatment of the global system, where the whole system is divided into multiple sub-domains. To tackle the mixed separation interfaces between acoustic domains, a compound structure treatment is proposed, with the aperture being modeled as an equivalent structural component. As demonstrated later, the unified structural and acoustic component over a mixed interface provides an effective tool to handle multiple internal partitions.

In this paper, the formulation procedure of the proposed modeling framework is

first elaborated, along with the subsystem treatment. Using the model, the separate effects of several typical silencer configurations are considered, which include: a) side-branch cavities with horizontal partitions/extensions; b) multi-chamber silencer with vertical partitions; c) non-symmetric inlet and outlet. The combined effects of the above configurations are then analyzed. The accuracy and convergence of the method are verified against FEM results. Physical phenomena corresponding to different configurations are investigated in detail through visualizing the internal pressure field. An experimental validation on a dual-chamber silencer with horizontal partitions is also conducted, showing a good agreement with theoretical predictions.
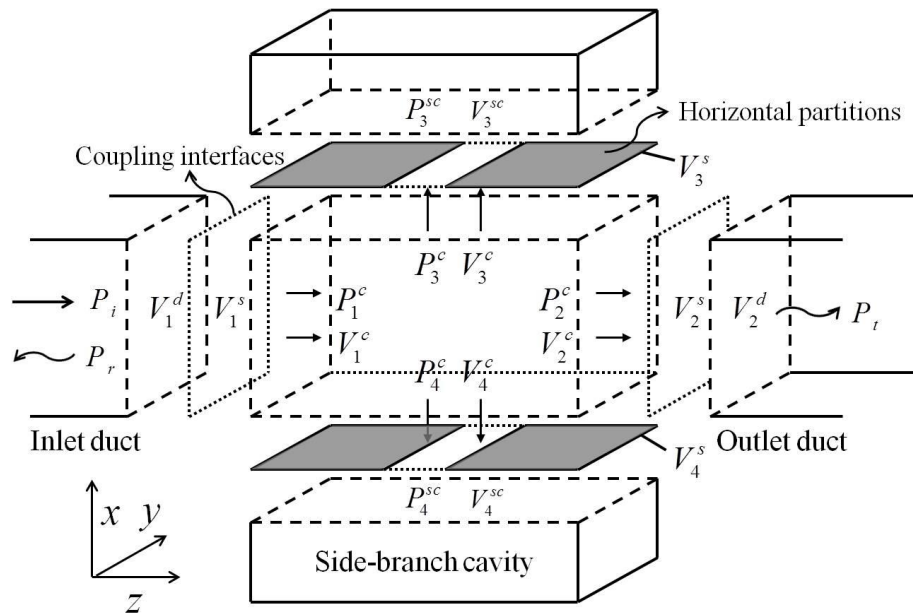
2. Formulation

Fig. 2. Sub-structuring treatment of a 3-D rectangular expansion chamber with side-branch cavities covered by partial partitions.

The detailed formulation procedure, along with the treatment of subsystem patch

transfer functions (PTFs), is illustrated using a silencer example as shown in Fig. 2. The chamber expansion volume is separated by two pairs of extensions at the inlet and outlet, allowing air apertures directly connecting the side-branch cavities and the main duct. The sub-divided acoustic domains, namely the inlet/outlet ducts and two side-branch cavities, are connected via four separation interfaces to the main chamber.

According to the PTF formulation, each interface area S is first meshed into N elementary rectangular surfaces called "patches", whose dimension is kept smaller than half of the minimum acoustic wavelength of interest to ensure the calculation convergence [15,16]. The excitation-response relationship between patches at each connecting interface is characterized using the corresponding subsystem PTFs:

$$
\begin{aligned}
&\textit{Structural}: \quad Y^s = \frac{\overline{V_i^s}}{\overline{F_j^s}}, \quad \textit{where} \quad \overline{V_i^s} = \frac{1}{S_i} \int_{s_i} V^s dS_i \quad \textit{and} \quad \overline{F_j^s} = \frac{1}{S_j} \int_{s_j} F^s dS_j \\
&\textit{Acoustical}: \quad Z^a = \frac{\overline{F_i^a}}{\overline{V_j^a}}, \quad \textit{where} \quad \overline{V_j^a} = \frac{1}{S_j} \int_{s_j} V^a dS_j \quad \textit{and} \quad \overline{F_i^a} = \int_{s_i} P^a dS_i
\end{aligned}
\tag{1}
$$

where subscripts i and j denote the receiving and exciting patch, S_i, S_j denote the corresponding surface area. For structural subsystems such as vibrating plates, patch mobility Y^s is generally used, while for acoustical subsystems, using patch impedances Z^a is more convenient. Note that the velocities and forces at all the sub-divided patches are averaged quantities.

In principle, if the four coupling surfaces numbered from 1 to 4 can be characterized using pure vibrating "structural" interfaces (even in the presence of air aperture), the system can be described based on the superposition principle of linear vibroacoustic system as follows [16]:

$$Y_1^s(\tilde{F} + Z_1^d V_1^d + Z_{11}^c V_1^c + Z_{12}^c V_2^c + Z_{13}^c V_3^c + Z_{14}^c V_4^c) = V_1^s$$
$$Y_2^s(Z_2^d V_2^d + Z_{21}^c V_1^c + Z_{22}^c V_2^c + Z_{23}^c V_3^c + Z_{24}^c V_4^c) = V_2^s$$
$$Y_3^s(Z_{31}^c V_1^c + Z_{32}^c V_2^c + Z_{33}^c V_3^c + Z_3^{sc} V_3^{sc} + Z_{34}^c V_4^c) = V_3^s \qquad (2)$$
$$Y_4^s(Z_{31}^c V_1^c + Z_{32}^c V_2^c + Z_{43}^c V_3^c + Z_{44}^c V_4^c + Z_4^{sc} V_4^{sc}) = V_4^s$$

where Y^s, V^s represent the structural mobilities and vibrating velocities of the four "structural" interfaces, $Z^d, V^d, Z^c, V^c, Z^{sc}, V^{sc}$ are the acoustic impedances and velocities of the inlet/outlet duct, main chamber, and side-branch cavities, respectively. $\tilde{F}$ is the excitation force at the entrance of the silencer.

For conventional subsystems, the calculation of PTFs is rather straightforward based on the modal expansion theory, while the remaining challenge mainly comes from the modeling of the mixed separation with air aperture. To determine all the frequency-dependent dynamic terms embedded in Eq. (2), the following sub-sections present the detailed formulation of this compound structural subsystem and PTFs of other necessary subsystems.

2.1 Patch mobility of compound structure

The "structuralized" treatment of a pure air aperture is formulated as follows: consider an aperture connecting the two acoustic domains having a thin thickness of L_a, its internal pressure field can be expanded analytically in terms of propagating and evanescent acoustic modes:

$$p_a(x, y, z) = \sum_n a_a^n \psi_a^n (e^{-jk_z^n z} + \hat{\varepsilon}^n e^{jk_z^n z})$$

$$\psi_a^n(x, y) = \cos(\frac{n_x \pi}{L_x^a} x)\cos(\frac{n_y \pi}{L_y^a} y), \ n_x, n_y = 0,1,2 \cdots \qquad (3)$$

where the *z-axis* depicts the aperture thickness direction; a_a^n the *n*-th modal

amplitude of the aperture, $\psi_a^n(x,y)$ the cross-sectional eigenfunction of rectangular aperture; $\hat{\varepsilon}^n$ the coefficient ratio between the acoustic waves in the positive and negative z direction; $k_z^n = \sqrt{(\omega/c_0)^2 - k_x^2 - k_y^2}$ the corresponding wavenumber in the z-axis; the series indices n_x and n_y need to be truncated to a sufficient number to ensure the calculation convergence.

The small aperture thickness compared to the acoustic wavelength of interest delimits its velocity fluctuation in the z direction. Thus, an averaged through-thickness velocity can be assumed by using the pressure gradient at the front surface (z=0), and the sound pressures at the back surface (z=L_a) can be expressed using a Taylor's series expansion with neglected second-order higher terms [19]:

$$\bar{V}_z = \frac{1}{-j\rho_0\omega}\frac{\partial p_a}{\partial z} = \sum_n \frac{a_a^n k_z^n (1-\hat{\varepsilon}^n)\psi_a^n}{\rho_0\omega}$$

$$p_a(x,y,L_a) \approx p_a(x,y,0) + L_a\frac{\partial p_a}{\partial z}$$

(4)

Given a pressure disturbance $\Delta p = p_a(x,y,0) - p_a(x,y,L_a)$ acting on both sides of the aperture, and making use of the modal orthogonality property, the aperture modal amplitude can be calculated as:

$$jk_z^n L_a a_a^n (1-\hat{\varepsilon}^n)N_a^n = \int_{S_a} \Delta p \psi_a^n dS_a$$

(5)

where $N_a^n = \int_{S_a} \psi_a^n \psi_a^{n'} dS$.

Then, according to the definition of structural mobility in Eq. (1), the equivalent aperture patch mobility Y^a can be obtained as:

$$Y^a = (\frac{1}{j\rho_0\omega L_a s_i s_j})\sum_n \frac{1}{N_a^n}\int_{S_i}\psi_a^n dS_i \int_{S_j}\psi_a^n dS_j$$

(6)

It can be seen that the aperture modeling in the present form can be fully viewed as a vibrating panel, where the equivalent structural properties such as the panel thickness, density, rigidity, and introduced damping are embedded [19]. Note that the proposed aperture treatment is, in principle, not limited to rectangular apertures, while other geometries are still applicable as long as the eigenfunction ψ_a^n can be obtained somehow. At its current version, however, the treatment only applies to flat separation interfaces due to the mathematical handling along the thickness direction.

On the other hand, the modeling of the flexural structure of the compound interface does not pose any technical difficulty, whose structural patch mobility can be easily determined [16]. The dynamic response of a compound structure under excitation can then be calculated by combining the plate mobility Y^p and aperture mobility Y^a into a single mobility matrix:

$$\begin{bmatrix} Y^p & 0 \\ 0 & Y^a \end{bmatrix} \begin{Bmatrix} \overline{F}^p \\ \overline{F}^a \end{Bmatrix} = \begin{Bmatrix} \overline{V}^p \\ \overline{V}^a \end{Bmatrix} \tag{7}$$

where $\overline{F}^p$ and $\overline{F}^a$ are the excitation forces impinging on the panel and aperture surface, $\overline{V}^p$ and $\overline{V}^a$ are the vibrational velocities of the real plate and aperture, at each corresponding patch. The brought benefit using the present formulation is obvious: modeling different combinations of rigid/flexible structures and apertures among a mixed separation interface no longer requires tedious continuity treatments at different parts. Thus, the modular sub-structuring framework is maintained and the overall modeling effort can be greatly reduced.

2.2 Patch impedance of acoustic cavities

The main chamber of the silencer as seen from Fig. 2 can be considered as a classical acoustic cavity. As to its modeling, Green's formula together with Helmholtz equation is used for describing the enclosed sound pressure field:

$$\int_{V_c} (p_c \nabla^2 \varphi_c - \varphi_c \nabla^2 p_c) dV_c = \int_{s_c} (p_c \frac{\partial \varphi_c}{\partial n} - \varphi_c \frac{\partial p_c}{\partial n}) dS_c \tag{8}$$

The internal pressure field p_c is expanded analytically in terms of the rigid-walled acoustic modes of a rectangular cavity:

$$p_c(x, y, z) = \sum_r a_c^r \varphi_c^r$$

$$\varphi_c^r(x, y, z) = \cos(\frac{r_x \pi}{L_x^c} x) \cos(\frac{r_y \pi}{L_y^c} y) \cos(\frac{r_z \pi}{L_z^c} z), \ r_x, r_y, r_z = 0, 1, 2 \cdots \tag{9}$$

where a_c^r is the r-th modal amplitude of the cavity; φ_c^r is the corresponding mode shape function; r_x, r_y, r_z are the modal indices in the x, y, z directions.

By substituting the momentum equation $\frac{\partial p_c}{\partial n} = -j\rho_0 \omega \overline{V}_n$ into Eq. (8), the modal amplitude of the cavity due to a vibrating boundary is expressed as:

$$a_c^r N_c^r (k^2 - k_r^2) = \int_{s_c} (j\rho_0 \omega \overline{V}_n) \varphi_c^r dS_c \tag{10}$$

where $N_c^r = \int_{S_c} \psi_c^r \psi_c^{r'} dS_c$; the cavity resonances are $k_r = \sqrt{(\frac{r_x \pi}{L_x^c})^2 + (\frac{r_y \pi}{L_y^c})^2 + (\frac{r_z \pi}{L_z^c})^2}$.

Using the definition of acoustic impedance in Eq. (1), the patch impedance between a receiving patch i and an exciting patch j can be calculated as:

$$Z^c = \sum_r \frac{j\rho_0 \omega}{N_c^r (k^2 - k_r^2)} \int_{s_i} \varphi_c^r dS_i \int_{s_j} \varphi_c^r dS_j \tag{11}$$

In Fig. 2, the main chamber cavity is coupled to the surrounding acoustic domains through four vibrating boundaries. The exciting and receiving patches may come from

different surfaces. Thus, the self-surface and cross-surface impedances are to be

specified, by using *m, n* to identify the surfaces where the receiving and exciting

patches are located,

$$Z_{mn}^c = \sum_r \frac{j\rho_0\omega}{N_c^r(k^2 - k_r^2)} \int_{S_m} \varphi_c^r dS_m \int_{S_n} \varphi_c^r dS_n \tag{12}$$

For example, Z_{14}^c represents the response at surface 1 due to a vibrating

excitation at surface 4. In total, 16 self- and cross- surface impedances are to be

calculated for constructing Eq. (2). The corresponding integrations of pressure

eigenfunctions at the four boundary surfaces are summarized as follows:

$$
\begin{aligned}
&surface \quad 1: \quad \int_{s_1} \varphi_r^c dS_1 = \int_{S_1} \cos(\frac{r_x\pi}{L_x^c} x)\cos(\frac{r_y\pi}{L_y^c} y)dS_1 \\[2mm]
&surface \quad 2: \quad \int_{s_2} \varphi_r^c dS_1 = \int_{S_2} (-1)^{r_z}\cos(\frac{r_x\pi}{L_x^c} x)\cos(\frac{r_y\pi}{L_y^c} y)dS_2 \\[2mm]
&surface \quad 3: \quad \int_{s_3} \varphi_r^c dS_3 = \int_{S_3} (-1)^{r_x}\cos(\frac{r_y\pi}{L_y^c} y)\cos(\frac{r_z\pi}{L_z^c} z)dS_3 \\[2mm]
&surface \quad 4: \quad \int_{s_4} \varphi_r^c dS_4 = \int_{S_4} \cos(\frac{r_y\pi}{L_y^c} y)\cos(\frac{r_z\pi}{L_z^c} z)dS_4
\end{aligned}
\tag{13}
$$

Special attention should be paid to the signs of the above patch impedances when

using Green's formula. In Eq. (2), the coupling equations of the system are established

according to the normal pressure and velocity notations prescribed in Fig. 2, but the

normal direction of Green's formula is conventionally prescribed as pointing outward.

Thus, an extra negative sign should be added to the cross-patch impedance during

calculation whenever these two notations are contradicted:

$$
\begin{aligned}
&Z_{11}^c \ (+);\ Z_{22}^c \ (+);\ Z_{12}^c \ (-);\ Z_{21}^c \ (-); \\
&Z_{33}^c \ (+);\ Z_{44}^c \ (+);\ Z_{34}^c \ (+);\ Z_{43}^c \ (+); \\
&Z_{13}^c \ (-);\ Z_{31}^c \ (-);\ Z_{14}^c \ (-);\ Z_{41}^c \ (-); \\
&Z_{23}^c \ (+);\ Z_{32}^c \ (+);\ Z_{24}^c \ (+);\ Z_{42}^c \ (+);
\end{aligned}
\tag{14}
$$

As to the modeling of the two side-branch cavities, their patch impedances Z_3^{sc} and Z_4^{sc} at the connecting surfaces to the main chamber can be formulated using exactly the same treatment. It is worth mentioning that the rigid-walled acoustic modes being used may slightly differ from the actual condition in the vicinity of the boundaries, where the normal velocity along the boundary is zero. It is commonly accepted that the rigid mode superposition gives very accurate estimation of the sound pressure across the interface, but not the velocity. That is the reason why the calculation of acoustic impedances (not mobilities) is adopted here. In the numerical examples, the convergence and accuracy of assuming these rigid mode expansions for cavity pressures will be demonstrated.

2.3 Patch impedance of inlet and outlet duct

Based on the modal expansion theory, the radiated sound pressure at the duct end due to a vibrating surface excitation can be expressed as:

$$p_d(x, y) = \sum_s a_d^s \Psi_d^s$$

$$\Psi_d^s(x, y) = \cos(\frac{s_x \pi}{L_x^d} x) \cos(\frac{s_y \pi}{L_y^d} y), \ s_x, s_y = 0, 1, 2 \cdots$$

(15)

where a_d^s is the s-th modal amplitude of the duct, $\Psi_d^s(x, y)$ is the corresponding planar eigenfunction.

Assuming a vibrating velocity $\overline{V}_n$ over the duct end surface, its modal amplitude a_d^s can be calculated as:

$$a_d^s = \rho_0 c_0 \sum_s \frac{1}{N_d^s \sin \theta} \int_{S_d} \overline{V}_n \Psi_d^s dS_d$$

(16)

where $N_d^s = \int_{S_d} \Psi_d^s \Psi_d^{s'} dS_d$; the modal phase angle which is frequency-dependent:

$$\sin\theta = -\sqrt{1 - \frac{[(s_x \pi / L_x^d)^2 + (s_y \pi / L_y^d)^2]}{(\omega / c_0)^2}} \ .$$

Again, according to the definition of acoustic patch impedance in Eq. (1), the duct radiation impedance between an exciting patch j and receiving patch i can be obtained as:

$$Z^d = \rho_0 c_0 \sum_s \frac{1}{N_d^s \sin\theta} \int_{S_i} \Psi_d^s dS_i \int_{S_j} \Psi_d^s dS_j \qquad (17)$$

2.4 Global system response and TL calculation

So far, PTFs of all the structural and acoustic subsystems have been formulated. Adding continuous velocity conditions at the four coupling surfaces to Eq. (2):

$$\begin{aligned} &V_1^d = V_1^s = V_1^c, V_2^c = V_2^s = V_2^d; \ at \ coupling \ surfaces \ 1, \ 2 \\ &V_3^c = V_3^{sc}, V_4^c = V_4^{sc}; \ at \ coupling \ surfaces \ 3, \ 4 \end{aligned} \qquad (18)$$

and assuming a plane wave excitation $\tilde{F}$ with unity pressure amplitude at the inlet, the fully coupled system equations can be rearranged into a more compact form as

$$[M]\{V\} = \{F\} \qquad (19)$$

where

$$M = \begin{bmatrix} Y_1^s(Z_1^d + Z_{11}^c) - I & Y_1^s Z_{12}^c & Y_1^s Z_{13}^c & Y_1^s Z_{14}^c \\ Y_2^s Z_{21}^c & Y_2^s(Z_2^d + Z_{22}^c) - I & Y_2^s Z_{23}^c & Y_2^s Z_{24}^c \\ Y_3^s Z_{31}^c & Y_3^s Z_{32}^c & Y_3^s(Z_{33}^c + Z_3^{sc}) - I & Y_3^s Z_{34}^c \\ Y_4^s Z_{31}^c & Y_4^s Z_{32}^c & Y_4^s Z_{43}^c & Y_4^s(Z_{44}^c + Z_4^{sc}) - I \end{bmatrix};$$

$$V = \{V_1^s \quad V_2^s \quad V_3^s \quad V_4^s\}; \qquad F = \{-Y_1^s \tilde{F} \quad 0 \quad 0 \quad 0\}$$

The patch velocity vector of the four coupling surfaces, obtained by solving the above equations, contains raw data of the system response, which can be post-processed to

evaluate the sound attenuation performance of an expansion chamber silencer. The TL is defined as $\mathrm{TL} = 20\log_{10}(1/\tau)$, where τ is the ratio between the transmitted and incident sound power. The incident sound power Π_i corresponding to a normal plane wave excitation with pressure amplitude p_0 is calculated as:

$$\Pi_i = \frac{|p_0|^2}{2\rho_0 c_0} \sum_{i=1}^{N} s_i \tag{20}$$

where N is the total number of patches over the inlet cross section. Similarly,

$$\Pi_t = \frac{1}{2}\sum_{i=1}^{N}\left(P_i^d\right)\left(V_i^d\right)^* s_i = \frac{1}{2}\sum_{i=1}^{N}\left(Z^d V_i^d\right)\left(V_i^d\right)^* s_i \tag{21}$$

where the asterisk denotes the complex conjugate of the patch velocity at the outlet.

3. Separate effects of different silencer configurations

3.1. Empty expansion chamber

3.2. Horizontal partitions/extensions

Partially covered side-branch cavities with rigid partitions, or typically referred to as extended inlet/outlet when the partitions are short [2, 3], are investigated. Using 1-D plane wave model, the analytical analysis (see Appendix) yields $f_r = nc_0/4L_{sc}$, $n = 1,3,5\ldots$ (L_{sc} is the horizontal length of the side-branch partition), where the TL is maximized due to the presence of extensions. At these frequencies, the side-branch cavities act as acoustic resonators, which counter the acoustic waves in the main stream at the conjunction of apertures, thus preventing their propagation to the downstream.
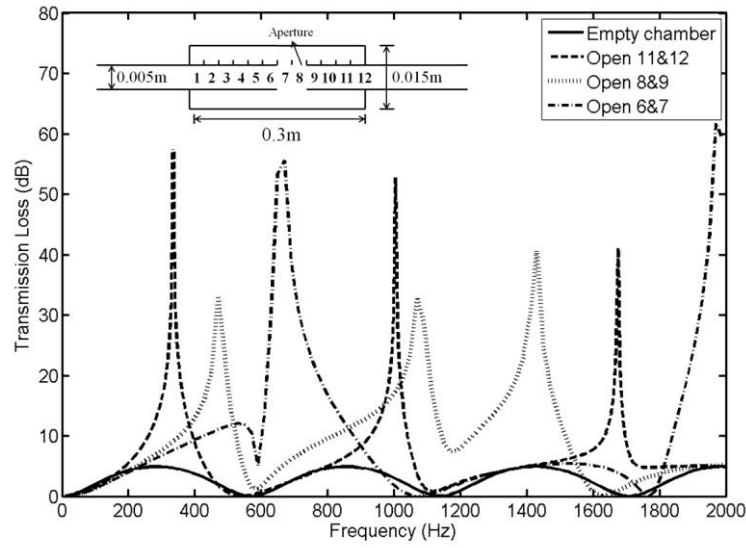
Fig. 4. Effect of horizontal partitions: very small cross-section.

The prediction and possible tuning of these TL peaks is important for silencer design in order to cope with a particular frequency range. In order to investigate this issue and to check the possible correlation between the 1-D analysis and the present 3-D model, two different duct configurations are examined. The first configuration involves a small cross-section, with reduced heights of the inlet/outlet ducts and the main chamber to $0.005m$ and $0.015m$, respectively, as shown in Fig.4. The relatively large length/height ratio helps reduce the effect of higher-order acoustic modes. To facilitate the treatment, the chamber length, being kept at $0.3m$, is evenly divided into 12 segments as shown in Fig. 4, where two segments are allowed to open at each time by assigning aperture patches to the corresponding positions. By doing so, the positions of the opening can be adjusted, whilst changing the lengths of the inlet/outlet extensions. In Fig. 4, the predicted TLs using the present approach are presented for three cases: apertures open at segments 11&12 (right end), 8&9, and 6&7 (center). It can be seen that the position of the opening can significantly affect

the TLs over the entire frequency region. In addition to the dome-like TL behavior, the extension adds sharp TL peaks due to the acoustic resonator effect. The positions of these TL peaks correlate well with the predictions using 1-D model [Eq. (A.4)], which indicates that 1-D model can be roughly used to tune the desired positions of generated TL peaks when the silencer's cross-section is small enough.
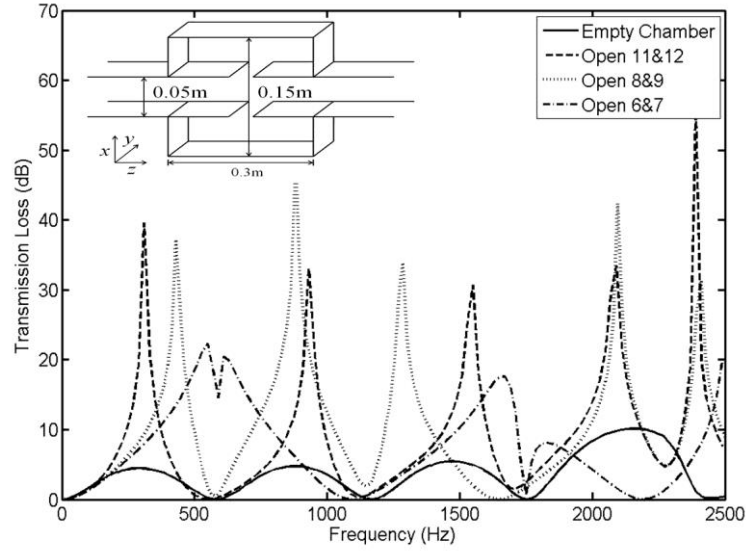

Fig. 5. Effect of horizontal partitions: normal cross-section dimension.

Similar analyses, with a larger cross-sectional dimension as the one used in Section 3.1, are conducted and shown in Fig. 5. Again, the combined effect of the expansion chamber and acoustic resonator is obvious. For the first case with apertures at the right end (patch 11&12 opened), the effective resonator frequencies closely coincide with the original TL domes, thus forming sharp and narrow TL stop-bands, but the zero-attenuation troughs are nearly unaffected. While for the third case with apertures in the middle (patch 6&7 opened), the first trough, attributed to the first chamber stream-wise mode, is lifted-up through the coupling with the side-branch,

resulting in a wider attenuation band below 1000 Hz. This indicates that, through a proper tuning of the side-branch length or the aperture position, the TL of an expansion chamber-type silencer can be significantly improved. On the other hand, the long extensions at the inlet and outlet help to alleviate the induced pressure drop due to the sudden expansion and contraction [8,9].

However, the previous 1-D theory is shown to be no longer accurate enough for predicting the TL peak positions of the current dimension, due to the inevitable 3-D effect. In Fig. 6, sound pressure distribution inside the silencer with aperture at outlet end is plotted at f=320 Hz, corresponding to its first TL peak. It is observed that the pressure nodal lines are not only determined by the horizontal length of the side-branch cavities, but also affected by the silencer height. To roughly estimate this frequency, geometric approximation can be used to account for the effect of silencer height, resulting in an increased resonator length $L'_{sc} = \sqrt{L_{sc}^2 + (0.5H)^2}$. Note that the reason of incorporating half silencer height $0.5H$ is due to the vertical geometric symmetry. This estimation yields a frequency of 325 Hz with L'_{sc}=0.26m, which is very close to the peak position on the TL curve. Similarly, when the aperture is placed in the middle, such estimation gives a reasonable prediction of first TL peak at 560Hz.
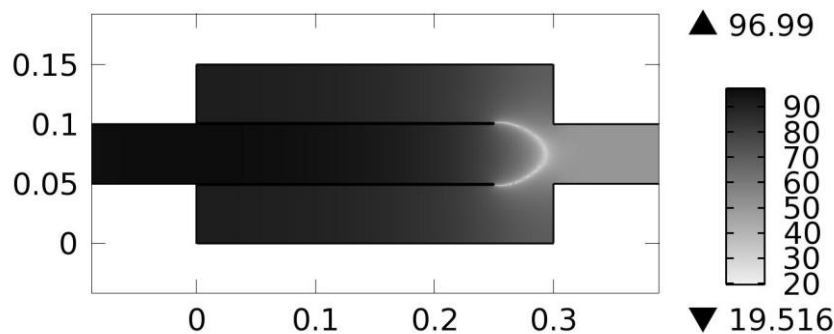

Fig. 6. Pressure level plot when the aperture is at right end, f=320Hz.

The above analyses suggest that the inlet/outlet extensions help enhance the sound attenuation by creating sharp TL peaks, while warranting an expected improvement in mean flow performance. For better silencer design, it is possible to estimate and tune the positions of the effective frequencies: for silencer with small cross-section whose cut-off frequency is far beyond the frequency range of interest, 1-D theory based on the side-branch length is accurate enough. While for larger silencers, 3-D modeling which takes the higher-order effects into account is necessary.

3.3. Multi-chamber silencer
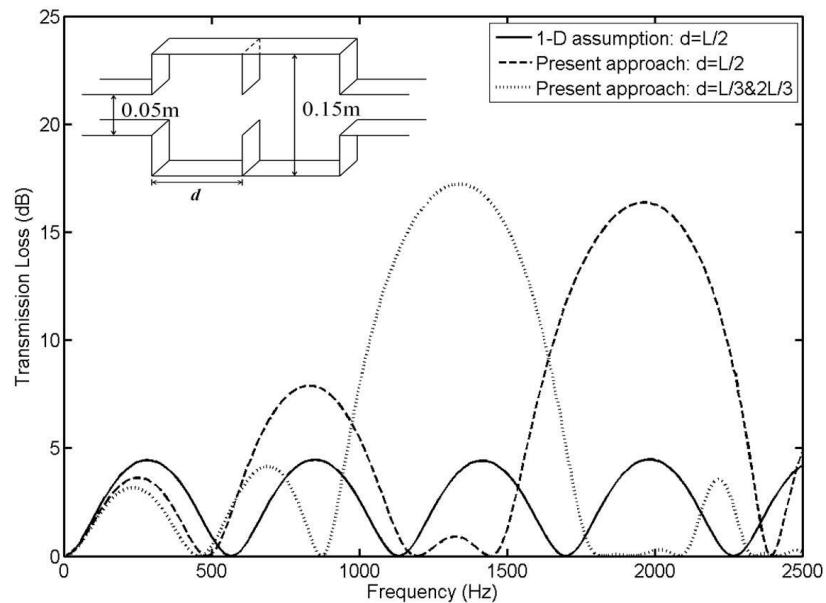
Fig. 7. Effect of adding vertical partitions.

The effect of multi-chambers by adding thin vertical partitions is studied in this section. Again, 1-D analytical analysis for silencer with small enough cross-section is first performed (see Appendix). The calculated TL plotted in Fig. 7 shows that the added vertical partitions have no influence on the attenuation performance under the

plane wave assumption. Using 3-D PTF model, however, the partitions vertically located at the center create a shift of the first and third TL troughs toward lower frequencies, resulting in a wider bandwidth and higher TL level of the second and forth dome. To explain the mechanism, the pressure field corresponding to the lowered trough at f=470 Hz is visualized in Fig. 8, which shows that the sound propagation from the inlet to the outlet exactly undergoes a half wavelength at this frequency. The air volume inside the chamber forms like a slightly bended conduit around the partition and the chamber walls, thus lengthening the characteristic length of the chamber. For the second trough at f=1150Hz, the partitions are placed at the original maximum pressure region of the empty chamber, thus exerting no influence on the pressure field and TL.
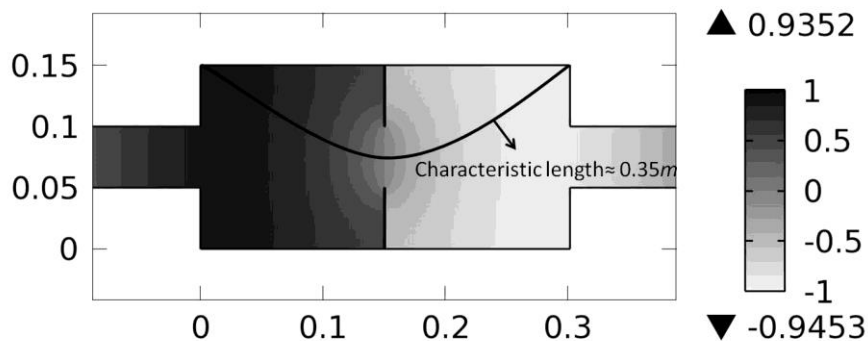
Fig. 8. Pressure field distribution inside the chamber with vertical partitions in the middle, the first trough is shifted from f=580Hz to f=470Hz.

Increasing the number of partitions will also provide additional room for tuning the silencing performance. This is shown in Fig. 7, where two pairs of partitions are inserted at $d=L/3$ and $2L/3$ simultaneously. It can be observed that the first two domes

are narrowed, whereas the bandwidth and TL levels of the third dome are increased. The visualized pressure fields indicate basically the same affecting mechanism as that observed in the previous case.

3.4. Asymmetric inlet/outlet orientation

The effect of non-symmetric layout on the TL, by offsetting the inlet and outlet ducts from the concentric center to the opposite corners, is studied. Using the proposed formulation, the positions where the inlet/outlet ducts are connected to the main chamber can be conveniently described. Figure 9 presents the calculated TL of an asymmetric chamber, which again shows excellent agreement with FEM result. It can be seen that the TL of the asymmetric chamber agrees well with the symmetric one below 700Hz, which indicates that the plane wave condition is still valid until this frequency. When multi-dimensional waves arise, the non-symmetric layout exhibits completely different acoustic behavior, with a sharp TL peak around the original second trough of the symmetric case.
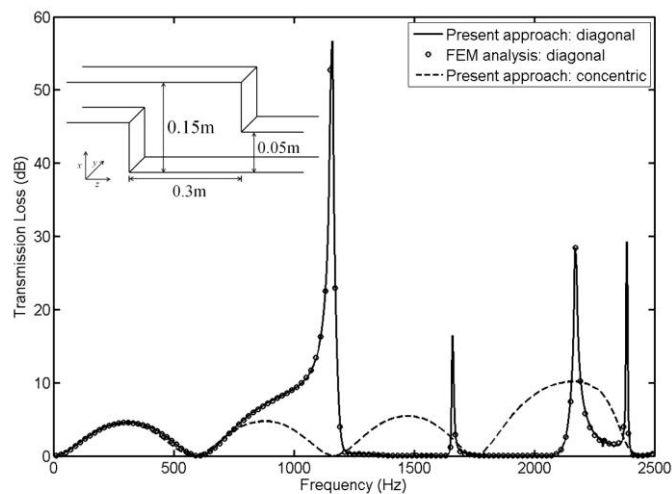

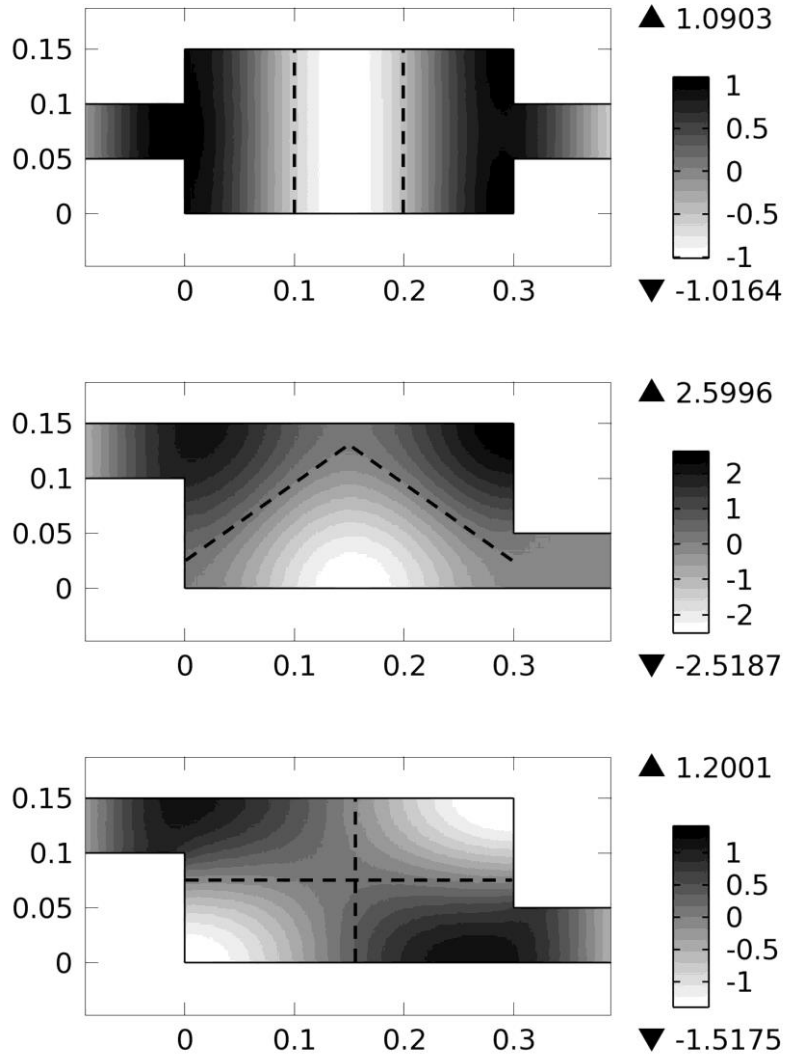Fig. 9. Effect of non-symmetric inlet and outlet.

Fig. 10. Pressure field distributions inside the chamber with approximate pressure nodal lines: a) symmetric, the second TL trough at f=1160Hz; b) asymmetric, the sharp TL peak at f=1160Hz; c) asymmetric, zero-attenuation starting from f=1260Hz.

In order to understand the observed sharp peak at f=1140 Hz, the sound pressure field, for both the symmetric and non-symmetric configurations, are compared at this particular frequency. As can be seen for the concentric case in Fig. 10(a), the zero-attenuation is due to the second chamber mode, where the nodal lines denoted by

the dashed lines are located at $L/3$ and $2L/3$. For the non-symmetric case in Fig. 10(b), however, the sound distribution combines the effects of the second horizontal mode and the first vertical mode (the height of the chamber is half of its length). The nodal lines show that the horizontal propagation is still dominant, but greatly affected by the vertical mode, resulting in high pressure regions at the left and right upper corners and an anti-phase high pressure region in the lower middle. By the same token, the outlet duct is a low sound pressure region, leading to a sharp TL peak with extremely high sound attenuation. When the frequency is increased to f=1260Hz, the pressure field plot in Fig. 10(c) shows a crossed modal pattern, which is rather similar to the first cross-mode (1,1) of a 2-D rectangular cavity of the same dimension. The outlet duct is thus exposed to the high pressure region, and provides negligible sound attenuation effect.

Although based only on a few selected configurations, the above analyses clearly shows that, by adopting different internal arrangement, the sound pressure distributions inside the duct at the expansion area can be manipulated and made use of. This provides considerable room for tuning and optimizing the performance of the expansion-type silencers for a give frequency range. For that, multi-dimensional sound propagation needs to be considered and 3-D modeling tools such as the one proposed in this paper is required.

4. Combined effects of silencer configurations

For practical silencer design, a single type of configuration as discussed in the

previous sections may not fulfill all the design requirements. Combining different configurations may bring about additional benefits, provided that the combined effects and the associated physical phenomena are clearly understood.

4.1. Asymmetric expansion chamber with internal partitions

In Fig. 11, vertical partitions (height=0.1m) are added to the asymmetric chamber used in Section 3.4. Two cases are considered: one partition in the middle $d=L/2$, and two staggered partitions at $d=L/3$ and $2L/3$. It can be seen from Fig.11 that, while basically maintaining similar TL pattern of the empty chamber, extra peaks are generated due to the added partitions, thus widening some of the attenuation bands. This leads to an improved overall silencing performance (except for low frequency range below 500Hz).
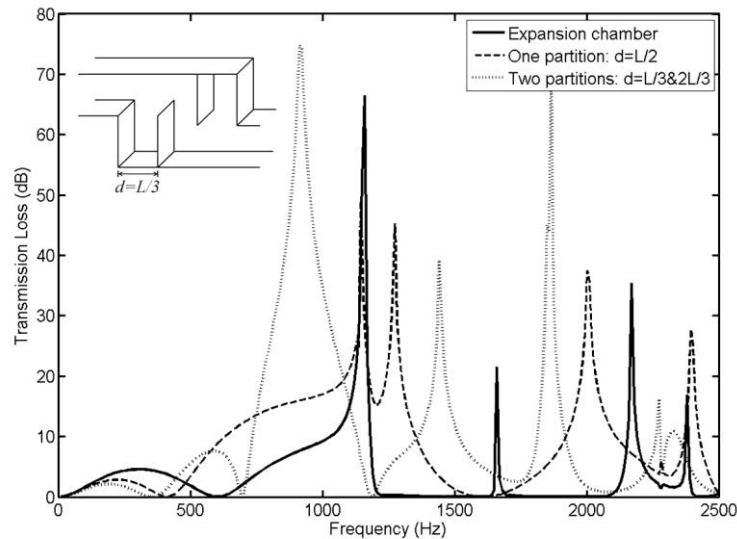

Fig. 11. Combined effect of asymmetric chamber with vertical partitions.

More specifically, for the case with one partition in the middle, the first TL trough is shifted toward lower frequency to f=400Hz. The underlying reason is due to an

increased characteristic chamber length, similar to that presented in Fig. 8. For the sharp TL peak at f=1160Hz, it can be seen from Fig. 12(a) that the acoustic pressure field, as well as the pressure nodal lines, are nearly unaffected compared to the empty chamber as plotted in Fig. 10(b). The reason is that the rigid partition is placed at the region where the acoustic pressure was maximum (pressure gradient equals to zero), thus exerting no influence on the original sound field. Right after this frequency, an extra TL peak at f=1260Hz appears, which lifts-up the acoustic pass-band of the empty chamber. Figure 12(b) shows that the rigid partition is placed at nodal line of the empty chamber (see Fig. 10(c)), thus greatly altering the original sound field. This leads to a significantly widened stop-band (with TL>10dB) from 600 to 1400Hz, compared to the narrow stop-band of the empty chamber. Similarly, with two staggered vertical partitions, the shifted resonances and the altered TL characteristics can also be explained in a similar manner by examining the locations of the partitions.
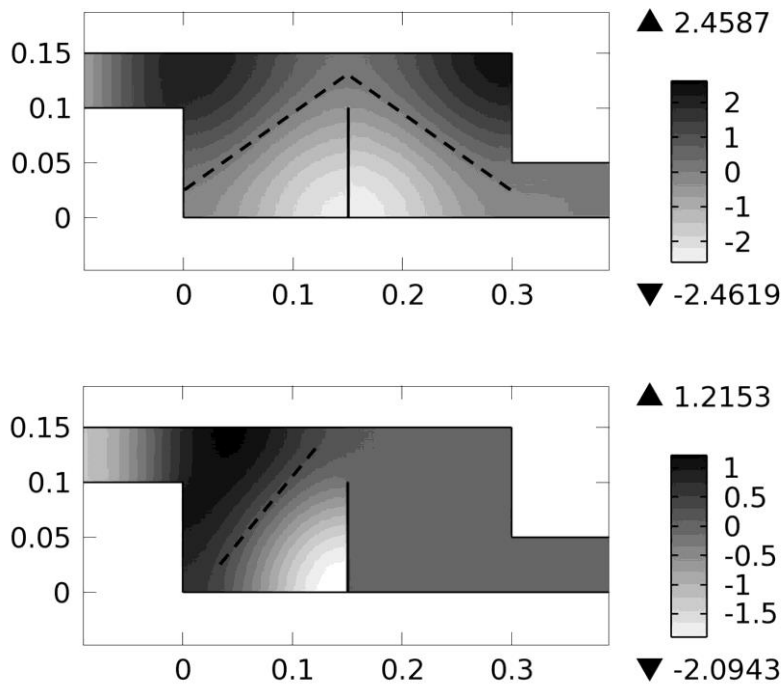
Fig. 12. Pressure field visualizations with approximate nodal lines: a) the first sharp peak at f=1160Hz; b) the second TL peak at f=1260Hz.

4.2. Multi-chamber silencer with horizontal partitions

The effect of combining multi-chambers with horizontal partitions is investigated. Using a three-chamber silencer as an example, Fig. 13 presents the TLs for three cases with the last two containing horizontal side-branch partitions. Case 1 is taken as benchmark for comparison. In Case. 2, inlet extension with a length of 0.08m is added to the first sub-chamber, which generates an extra TL peak at the original second dome (f=690Hz) and lifts-up the zero-attenuation after f=1800Hz as compared to Case 1. These contribute to the broadening of the mid-frequency stop-band from 1000~1600Hz to 600~1500Hz, and help to improve the TL performance at mid-high frequency range. Case 3 adds additional complexities to the system by adding extra horizontal extensions to the two remaining chambers. As illustrated in the sketch, extension inside the second chamber on the right is 0.02m in length, and the third chamber on the left is 0.06m. It can be seen that with a combination of different side-branch lengths, the predicted TL level is generally increased with multiple sharp peaks appearing along the frequency range. In Fig. 14(a), the sound pressure field at its first TL peak f=690Hz is plotted. As expected, the strong attenuation is mainly attributed to the resonator effect of the extension inside the first sub-chamber, which explains the coincidence of TL peaks at this frequency for the two cases (2 and 3). In Fig. 14(b), the second TL peak at f=960Hz is plotted, which shows that the attenuation

is due to the extension inside the third sub-chamber. The medium and mid-high

frequency stop-bands are hereby changed to 500~1300Hz (bandwidth 800Hz) and

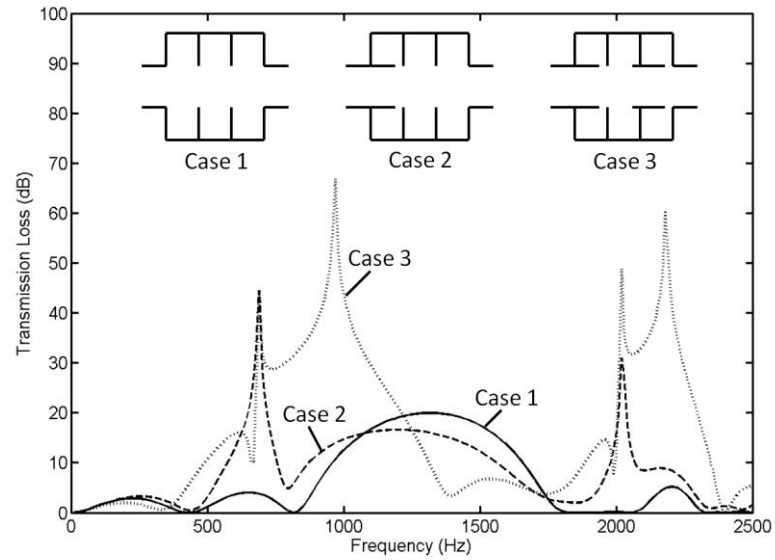1850Hz to 2350Hz (bandwidth 500Hz).

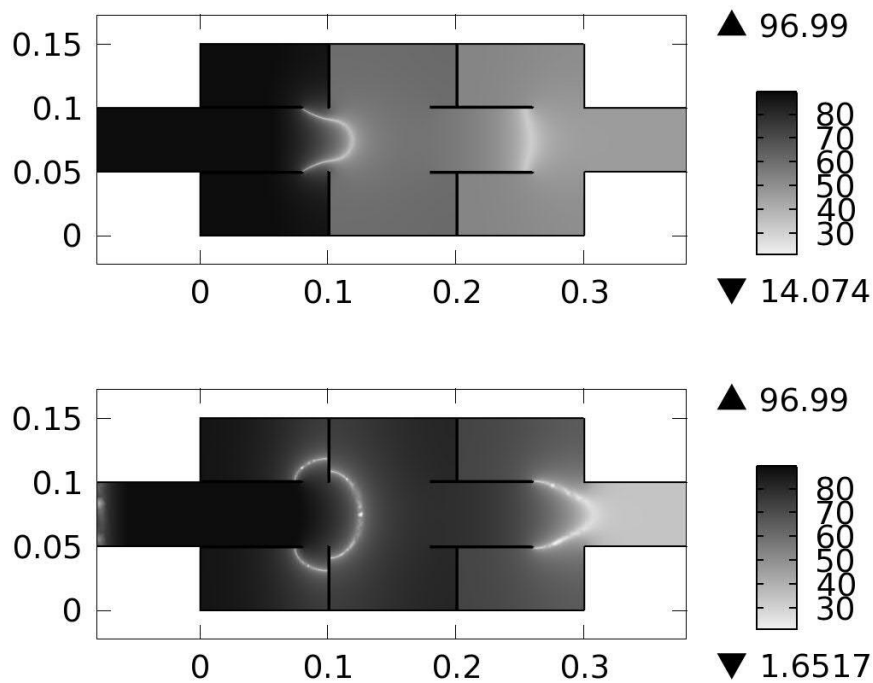Fig. 13. Combined effect of adding both vertical and horizontal partitions.

Fig. 14. Pressure level plots corresponding to Case. 3: a) the first TL peak at

f=690Hz; b) the second TL peak at f=960Hz.

It should be noted that the parameters used in all simulation examples, including the position and height of the internal partitions, the length and arrangement of the horizontal extensions, are randomly selected. No attempt was made to optimize the system. It can be anticipated that, due to the modular nature and the flexibility offered by the proposed formulation, the sound attenuation performance of such silencers can be further improved by tuning these parameters. As an even more general remark, it is relevant to note that the present compound structure formulation is not confined to mixed separations with only partitions and apertures. More complex configurations such as perforated/micro-perforated ducts, absorbing materials can also be apprehended basically following the same procedure [19].

5. Experimental validation

In order to validate the proposed formulation, the TL of a duct silencer, consisting of a dual-cell expansion chamber and side-branch partitions, is experimentally tested. As illustrated in Fig. 15, the measurement is conducted using the four-microphone method [21], where two pairs of 1/2-in. phase-matched microphones (B&K 4187) are used at the upstream and downstream, together with a conditioning amplifier (B&K Nexus 2691), to measure the acoustic pressures inside the duct. The cross-section of the inlet/outlet duct is $100mm \times 100mm$, and two independent experiments with different downstream loading conditions are used to simulate physical anechoic termination [21]. For the expansion chamber, two side-branch cavities with a height of $100mm$ and length of $300mm$ are attached to the mainstream, where a pair of

vertical partitions is placed in the middle with horizontal partitions of 160*mm* length. The vertical partitions made of 5*mm*-thick plates are sealed with rubber, and the four edges of the 1*mm*-thick horizontal partitions are inserted into the thin gap between the duct and side-cavity walls. The data acquisition system is controlled by an NI Labview program, running from 50Hz to 2000Hz with a step increment of 10Hz.
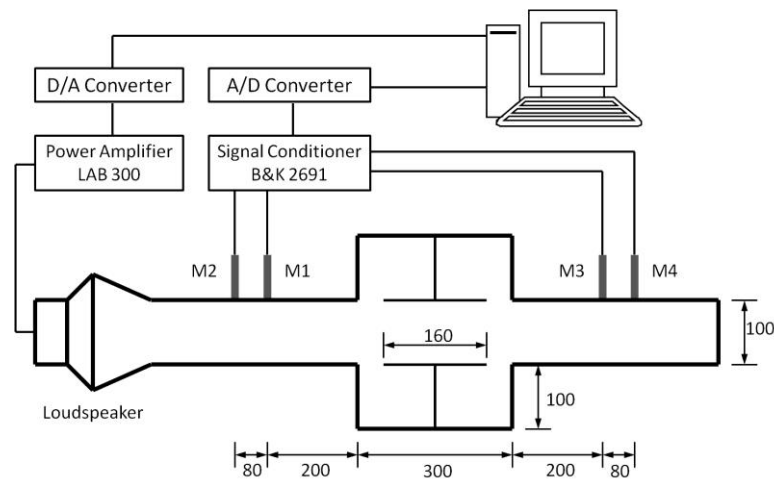

Fig. 15. Experimental setup, dimension in *mm.*

In the PTF simulation, all the partition walls are assumed to be acoustically rigid in the first place, and the damping loss factors for acoustic domains are taken as zero. The measured TL curve is compared with simulation in Fig. 16. The two curves show excellent agreement, except for some noticeable discrepancies at the first TL peak. Since the TL over 80dB is difficult to be captured in experiment [22], the discrepancies may come from the inherent limitation of the measurement. Another possible explanation is due to the vibration of the thin horizontal partitions being used, which was not apprehended in the simulation. In Ref. 23, Howard *et al.* also demonstrated experimentally that the structural-acoustic coupling may severely limit the silencing performance that can be achieved in reactive devices.
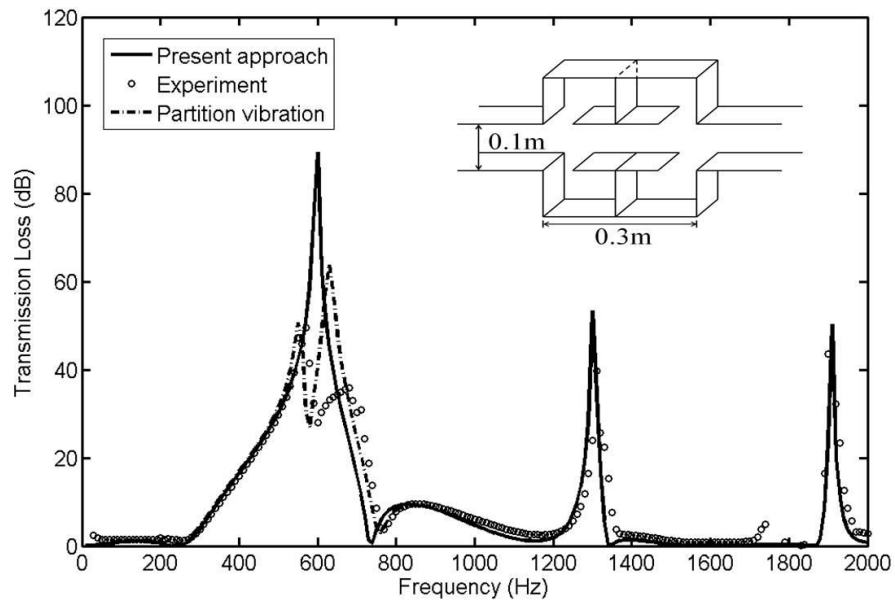
29

Fig. 16. Comparison of the predicted TLs (with/without consideration on the
horizontal partitions vibration) to the experimental measurement.

Since the proposed PTF approach is capable of dealing with panel vibration over
a mixed separation, the effect of possible flexural vibration of the horizontal partitions
is studied. With the consideration of the panel vibration (assumed as simply supported
for the sake of simplicity), the calculated TL as presented in Fig. 16 shows better
agreement with the experiment. In fact, the vibration of the panels indeed splits the
original TL peak, similar to the experimental curve, despite the remaining differences
in magnitude. Overall speaking, the PTF approach is validated with very satisfactory
accuracy using this example.

6. Conclusions

A sub-structuring formulation based on the PTF approach is proposed to deal

with reactive silencers involving complex internal layouts. The coupling description between the sub-divided acoustic domains is facilitated by the "compound structure" treatment for mixed separations. This treatment allows unifying the structural and acoustic interfaces into a single compound one, forming a more convenient description of the system. Through various examples and supported by comparisons with FEM and experimental results, the method is shown to be flexible, versatile and accurate to deal with various structural complexities inside silencers.

The proposed formulation has been applied to investigate the separate effects of several typical silencer configurations, including the side-branch partitions, multi-chamber partitions, and non-symmetric layout. Comparing with a simple expansion chamber, the introduced side-branch partitions greatly enhance the sound attenuation by combining the expansion effect and the acoustic resonator effect, and by the same token improve the flow performance. The positions of the generated TL peaks can be roughly estimated using an effective resonator length. The presence of vertical partitions generally leads to an improved TL and wider stop-bands for particular domes on the TL curve, where the shifted resonances can be explained and predicted by the bended air volume enclosed by the partition and the duct walls. The asymmetric inlet/outlet layout has negligible influence on the TL well below the cut-off frequency, but results in a drastically different TL behavior after the onset of higher-order modes. In addition, the combined effects of these configurations have also been studied, where the combination of different internal configurations generally provides additional benefits. The analytical predictions have shown

consistent agreements with FEM results throughout the analyses.

Although the analyses carried out in this study only involve a few selected configurations, it is obvious that, by adopting different internal arrangements, the sound pressure distributions inside the duct can be manipulated and made use of. This provides considerable room for tuning and optimizing the performance of the expansion-type silencers to satisfy the prescribed design criterion. For that, multi-dimensional sound propagation needs to be considered and 3-D modeling tools such as the one proposed in this paper are definitely needed. In addition, a thorough physical understanding on the effect of different internal arrangements is a critical aspect that will lead to a better acoustic design.

Appendix. Plane wave model for silencer with internal partitions

The effect of covering side-branch cavity with rigid extension in Section 3.2 is studied using a plane wave model, to understand its mechanism in generating TL peaks to an empty expansion chamber.
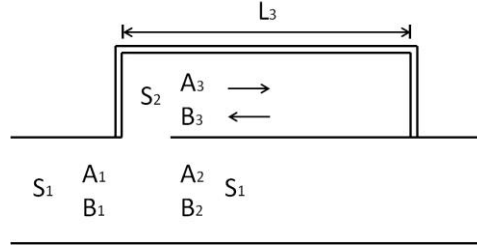

Fig. 17. Plane wave model for an expansion chamber with side-branch partition.

The forward and backward sound pressure coefficients for the inlet, outlet and side-branch cavity are as denoted in Fig. 17. The pressures and velocities at the conjunction of the aperture are related as:

$$A_1 + B_1 = A_2 + B_2 = A_3 + B_3$$
$$S_1(A_1 - B_1) = S_2(A_3 - B_3) + S_1(A_2 - B_2)$$

(A.1)

The rigid boundary condition at the rigid end of the side-branch and the anechoic termination for the outlet duct yield:

$$A_3 e^{-jkL_3} - B_3 e^{jkL_3} = 0$$
$$B_2 = 0$$

(A.2)

Combining the above equations gives:

$$\frac{A_1}{A_2} = 1 + \frac{S_2(e^{2jkL_3} - 1)}{2S_1(e^{2jkL_3} + 1)}$$

(A.3)

The transmitted pressure is infinite small when $2jkL_3 = n\pi$, $n = 1,3,5\cdots$, thus:

$$f_r = \frac{nc_0}{4L_3}, n = 1,3,5\cdots$$

(A.4)

On the other hand, to yield a TL peak at a certain frequency, the length of the side-branch cavity is required to be $L_3 = {nc_0}/{4f}$.

As to the effect of vertical partition in Section 3.3, the 1-D analysis is shown in Fig. 18, where the acoustic domain decomposition and the corresponding wave amplitudes are as depicted.
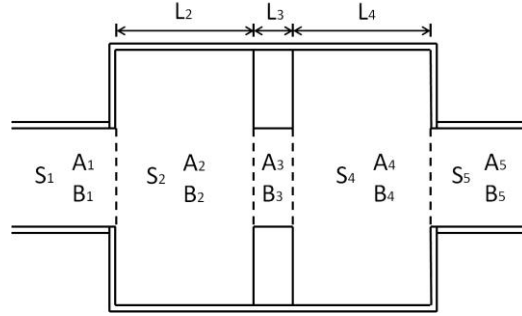

Fig. 18. Plane wave model for a silencer with a pair of vertical partitions.

At the four interfaces, the continuity conditions of acoustic pressures and velocities are written as:

$$
\begin{aligned}
S_{12}: \quad & A_1 + B_1 = A_2 + B_2 \\
& S_1(A_1 - B_1) = S_2(A_2 - B_2) \\
S_{23}: \quad & A_2 e^{-jkL_2} + B_2 e^{jkL_2} = A_3 + B_3 \\
& S_2(A_2 e^{-jkL_2} - B_2 e^{jkL_2}) = S_1(A_3 - B_3) \\
S_{34}: \quad & A_3 e^{-jkL_3} + B_3 e^{jkL_3} = A_4 + B_4 \\
& S_1(A_3 e^{-jkL_3} - B_3 e^{jkL_3}) = S_2(A_4 - B_4) \\
S_{45}: \quad & A_4 e^{-jkL_4} + B_4 e^{jkL_4} = A_5 + B_5 \\
& S_2(A_4 e^{-jkL_4} - B_4 e^{jkL_4}) = S_1(A_5 - B_5)
\end{aligned}
\tag{A.5}
$$

Solving coefficient A_5 with anechoic termination condition $B_5 = 0$ and a given inlet wave amplitude A_1, the TL can be calculated as $TL = 20\log_{10}\left|\dfrac{A_1}{A_5}\right|$.

REFERENCES

1. A. Selamet, P. M. Radavich, The effect of length on the acoustic attenuation performance of concentric expansion chambers: an analytical, computational and experimental investigation. *Journal of Sound and Vibration* **201** (1997) 407-426.

2. M. Åbom, Derivation of four-pole parameters including higher order mode effects for expansion chamber mufflers with extended inlet and outlet. *Journal of Sound and Vibration* **137** (1990) 403-418.

3. A. Selamet, Z. L. Ji, Acoustic attenuation performance of circular expansion chambers with extended inlet/outlet. *Journal of Sound and Vibration* **223** (1999) 197-212.

4. L. Huang, Broadband sound reflection by plates covering side-branch cavities in a duct. *The Journal of the Acoustical Society of America* **119** (2006) 2628-2638.

5. C. Q. Wang, L. Cheng, L. Huang, Realisation of a broadband low frequency plate silencer using sandwich plates. *Journal of Sound and Vibration* **318** (2008) 792-808.

6. J. W. Lee, Y. Y. Kim, Topology optimization of muffler internal partitions for improving acoustical attenuation performance. *International journal for numerical methods in engineering* **80** (2009) 455-477.

7. J. W. Lee, G. W. Jang, Topology design of reactive mufflers for enhancing their acoustic attenuation performance and flow characteristics simultaneously. *International Journal for Numerical Methods in Engineering* **91** (2012) 552-570.

8. J. M. Middelberg, T. J. Baber, S. S. Leong, K. P. Byrne, E. Leonardi,

Computational fluid dynamics analysis of the acoustic performance of various simple expansion chamber mufflers, *Proceedings of Acoustics* 2004 Australia

9. A. Selamet, F. D. Denia, A. J. Besa, Acoustic behavior of circular dual-chamber mufflers. *Journal of Sound and Vibration* **265** 2003 967-985.

10. R. Kirby, Simplified techniques for predicting the transmission loss of a circular dissipative silencer. *Journal of Sound and Vibration* **243** (2001) 403-426.

11. F. D Denia, A. Selamet, F. J. Fuenmayor, R. Kirby, Acoustic attenuation performance of perforated dissipative mufflers with empty inlet/outlet extensions. *Journal of Sound and Vibration* **302** (2007) 1000-1017.

12. T. W. Wu, G. C. Wan, Muffler performance studies using a direct mixed-body boundary element method and a three-point method for evaluating transmission loss. *Journal of Vibration and Acoustics* **118** (1996) 479-484.

13. M. C. Chiu, Shape optimization of multi-chamber mufflers with plug-inlet tube on a venting process by genetic algorithms. Applied Acoustics 71 (2010) 495-505.

14. A.Mimani, M.L.Munjal, Transverse plane wave analysis of short elliptical chamber mufflers: An analytical approach, *Journal of Sound and Vibration* **330** (2011) 1472-1489.

15. M. Ouisse, L. Maxit, C. Cacciolati, J. L. Guyader, Patch transfer functions as a tool to couple linear acoustic problems, *The Journal of the Acoustical Society of America* **127 (2005)** 458-466.

16. J. D. Chazot, J. L. Guyader, Prediction of transmission loss of double panels with a patch-mobility method, *The Journal of the Acoustical Society of America* **121 (2007)**

267-278.

17. L. Maxit, C. Yang, L. Cheng, J. L. Guyader, Modeling of micro-perforated panels in a complex vibro-acoustic environment using patch transfer function approach, *The Journal of the Acoustical Society of America* **131** (2012) 2118-2130.

18. X. Yu, L. Cheng, J. L. Guyader, Vibroacoustic modeling of cascade panels system involving apertures and micro-perforated elements, Conference paper, **20th** International Congress on Sound & Vibration (2013)

19. X. Yu, L. Cheng, J. L. Guyader, On the modeling of sound transmission through a mixed separation of flexible structure with aperture, *The Journal of the Acoustical Society of America* **135** (2014) 2785-2796

20. A. Selamet, N. S. Dickey, J. M. Novak, The Herschel–Quincke tube: a theoretical, computational, and experimental investigation. *The Journal of the Acoustical Society of America* **96** (1996) 3177-3185.

21. X. N. Wang, Y. S. Choy, L. Cheng, Hybrid noise control in a duct using a light micro-perforated plate. *The Journal of the Acoustical Society of America* **132** (2012) 3778-3787.

22. M. Wu, Micro-perforated panels for duct silencing. *Noise Control Engineering Journal* **45** (1997) 69-77.

23. C. Q. Howard, B. S. Cazzolato, C. H. Hansen, Exhaust stack silencer design using finite element analysis, *Noise Control Engineering Journal* **48** (2000) 113-120.

Figure Captions

Fig. 1. (a) An example of reactive silencers with complex internal partitions (b) Using

sub-structuring technique, the system is divided into uncoupled subsystems.

Fig. 2. Sub-structuring treatment of a 3-D rectangular expansion chamber with

side-branch cavities covered by partial partitions.

side-branch cavities covered by partial partitions.

Fig. 3. TL of a simple expansion chamber.

Fig. 4. Effect of horizontal partitions: very small cross-section.

Fig. 5. Effect of horizontal partitions: normal cross-section dimension.

Fig. 6. Pressure level plot when the aperture is at right end, f=320Hz.

Fig. 7. Effect of adding vertical partitions.

Fig. 8. Pressure field distribution inside the chamber with vertical partitions in the

middle, the first trough is shifted from f=580Hz to f=470Hz.

Fig. 9. Effect of non-symmetric inlet and outlet.

Fig. 10. Pressure field distributions inside the chamber with approximate pressure

nodal lines: a) symmetric, the second TL trough at f=1160Hz; b) asymmetric, the

sharp TL peak at f=1160Hz; c) asymmetric, zero-attenuation starting from f=1260Hz.

Fig. 11. Combined effect of asymmetric chamber with vertical partitions.

Fig. 12. Pressure field visualizations with approximate nodal lines: a) the first sharp

peak at f=1160Hz; b) the second TL peak at f=1260Hz.

Fig. 13. Combined effect of adding both vertical and horizontal partitions.

Fig. 14. Pressure level plots corresponding to Case. 3: a) the first TL peak at f=690Hz;

b) the second TL peak at f=960Hz.

Fig. 15. Experimental setup, dimension in *mm.*

Fig. 16. Comparison of the predicted TLs (with/without consideration on the horizontal partitions vibration) to the experimental measurement.

Fig. 17. Plane wave model for an expansion chamber with side-branch partition.

Fig. 18. Plane wave model for a silencer with a pair of vertical partitions.